



ACSIS Atlantic Ocean medium resolution SST dataset: Reconstructed 5-day, 1/2-degree, Atlantic Ocean SST (1950-2014)

Simon David Paul Williams¹ | David I. Berry²

¹National Oceanography Centre, Liverpool, UK

²National Oceanography Centre, Southampton, UK

Correspondence

Simon David Paul Williams, National Oceanography Centre, Joseph Proudman Building, 6 Brownlow Street, Liverpool, L3 5DA, UK.

Email: sdwil@noc.ac.uk

Funding information

Natural Environment Research Council, Grant/Award Number: NE/N018044/1

Abstract

A new dataset, the ACSIS Atlantic Ocean medium resolution SST dataset, is presented. This new dataset spans the period 1950–2014 at a 5-day, 1/2-degree resolution and covers the Atlantic Ocean. The dataset is based on in situ sea surface temperature (SST) observations from the International Comprehensive Ocean-Atmosphere Data Set interpolated using Kriging to infill gaps and is available from the Centre for Environmental Data Analysis (CEDA) archive. Compared to existing datasets, the resolution is increased by a factor of 4 spatially and 6 temporally.

KEYWORDS

Atlantic Ocean, ICOADS, reconstruction, Sea Surface Temperature, SST, VOS

1 | INTRODUCTION

The sea surface temperature (SST) is a key essential climate variable (ECV, e.g. Bojinski *et al.*, 2014) and a key essential ocean variables (EOV, e.g. Lindstrom *et al.*, 2012), with observations and datasets of the SST used in many studies. These include, inter alia: climate monitoring reports (e.g. IPCC, 2014; Blunden *et al.*, 2019); boundary layer for

atmospheric/oceanographic model forcing (e.g. Dee *et al.*, 2011); validation and assessment of coupled models (e.g. Flato *et al.*, 2013); air–sea interaction studies; and ecosystem studies (Villegas-Hernández *et al.*, 2015).

Due to its widespread use and importance, simple gridded and statistically reconstructed/infilled datasets of the sea surface temperature have been created. These include datasets spanning the period ~1,850—present on a relatively coarse

This article was funded by a grant from UK Natural Environment Research Council (reference NE/N018044/1)

Dataset

Details of the dataset(s) referred to in the paper. Include at least the name of dataset, data centre, and DOI or other unique identifier. If you are unable to provide this information until after publication, please contact the editorial team to organise access for the reviewers. Where possible please also provide the following details:

Identifier: <http://dx.doi.org/10.5285/83b0cd7e7cc6495a90b4cb967ead3577>

Creator: Williams, Simon D.P; Berry, David I.

Title: ACSIS Atlantic Ocean medium resolution SST dataset: Reconstructed 5-day, 1/2 degree, Atlantic Ocean SST (1950-2014)

Publishers: Centre for Environmental Data Analysis (Ceda)

Publication Year: 2020

Resource Type: dataset and metadata

Version: 1.0

This is an open access article under the terms of the Creative Commons Attribution License, which permits use, distribution and reproduction in any medium, provided the original work is properly cited.

© 2020 The Authors. Geoscience Data Journal published by Royal Meteorological Society and John Wiley & Sons Ltd

resolution (e.g. Rayner *et al.*, 2003; Hirahara *et al.*, 2014; Huang *et al.*, 2017; Kennedy *et al.*, 2019) and datasets spanning the satellite era (~1980 – present) at higher resolutions (e.g. Merchant *et al.*, 2014, 2019). The longer datasets typically have a monthly resolution and a spatial resolution of either 1° or 5°, with all the datasets based on the observations available within the International Comprehensive Ocean-Atmosphere Data Set (ICOADS, Freeman *et al.*, 2017). The primary differences between datasets are the treatment of biases in the observations and the infilling/gridding methods used. This dataset (ICOADS) is discussed further in Section 2, including known problems with the data. The datasets spanning the recent past typically have much higher resolution; for example, the recent European Space Agency (ESA) Climate Change Initiative (CCI) SST dataset (Merchant

et al., 2014, 2019) has a daily temporal resolution and 1/20° spatial resolution. These datasets are typically based on satellite data.

While the resolution of models (oceanographic, atmospheric, coupled) has increased with computing power, the resolution of gridded SST products, particularly those that extend before 1980, has largely remained static. This is due to inadequate sampling over large regions of the global oceans prior to the satellite era. While the sampling does not justify higher resolution products over much of the global oceans, the North Atlantic is an exception. In this region, the sampling density is much higher due to the density of shipping lanes and trade between Europe and the rest of the world (e.g. see Figure 1). In this paper, we describe a new SST dataset, making use of the increased

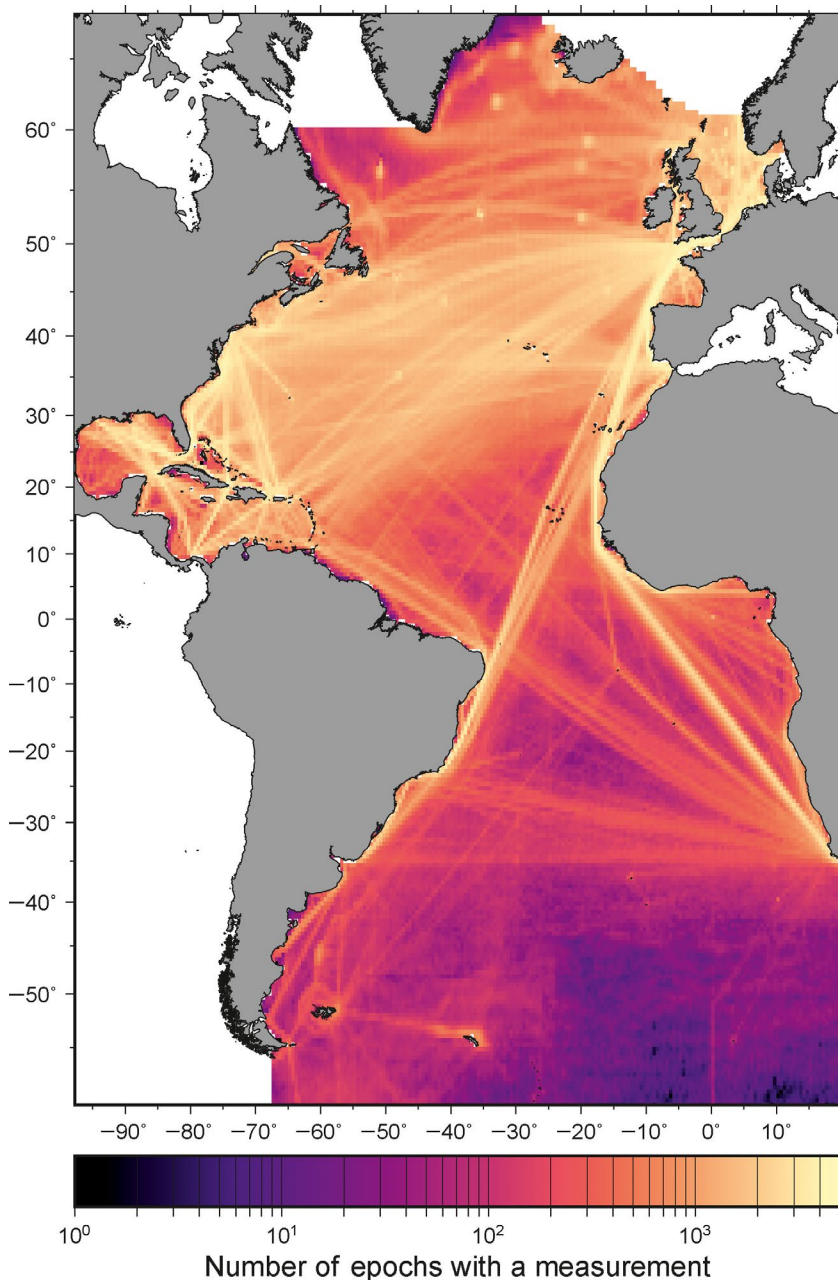


FIGURE 1 Map of the Atlantic Ocean showing the number of pentads with a measurement for each grid cell. Maximum number of pentads is 4,748

sampling to produce an intermediate resolution dataset for the Atlantic. The new dataset, ‘ACSIS Atlantic Ocean medium resolution SST dataset’, contains spatially interpolated estimates of the sea surface temperature on a 0.5° spatial grid, 5-day temporal resolution and spans the period 1950 – 2014. Section 2 describes the source observations and interpolation methods. Section 3 provides information on the new dataset, its location and format. Section 4 describes uses of the dataset and its limitations.

2 | DATA PRODUCTION METHODS

2.1 | Input data, spatial domain and data selection

2.1.1 | Input data

The new dataset described in this paper is based on the SST observations available from the ICOADS Release 3 (ICOADS R3.0 hereafter; Freeman *et al.*, 2017). The ICOADS R3.0 contains weather reports made on board ships, including the upper ocean, spanning the period ~1650–2014. Data from other platforms, for example drifting buoys, are also included. A near real-time (NRT) update to ICOADS, ICOADS R3.0.1, is available but there have been issues with the data included in this update (Freeman *et al.*, 2019). Consequently, only R3.0 has been used. Once the issues with the NRT update have been resolved, an updated version of the new dataset described in this paper will be produced.

The early weather reports in ICOADS are typically based on visual observations of the weather (present weather, wind force, sea state, ice), with instrumental observations (air temperature, sea temperature, pressure) beginning in the mid-19th century. More recently, the observations have included instrumental observations of wind speed and humidity. Beginning in the late 1980s and early 1990s, there are an increasing number of drifting buoy observations, with the drifting buoys dominating the in situ SST record from the mid-2000s onwards (e.g. Huang *et al.*, 2017).

The SST observations were made using a variety of methods, ranging from measuring the temperature of a sample of water collected in a canvas bucket, through engine intake measurements to infrared radiometric observations (Kent *et al.*, 2007), with the bucket and engine intake measurements the most common. Each method of observation has suffered from distinct biases and, as the methods used have changed over time, time varying biases exist in the raw data. For example, the measurements based on samples collected in buckets are biased cold due to cooling of the water sample in the buckets prior to measurement.

Similarly, the temperature measurements of water sampled from the engine cooling intake tend to be biased high due to heat from the engine room. Prior authors and dataset developers (e.g. Kennedy *et al.*, 2011a; Kennedy *et al.*, 2011b; Hirahara *et al.*, 2014; Huang *et al.*, 2017; Kennedy *et al.*, 2019) have applied bias corrections to reduce the impact of the biases on the climate record. A summary of the prior work on understanding and reducing the impact of these biases and the impact on the uncertainty in the SST climate record can be found in Kennedy (2014) and Kent *et al.* (2017). Recent work by others has included the examination of biases in different types of buckets (e.g. Carella *et al.*, 2017; Chan and Huybers, 2019).

Within the new dataset, nearly all observations for the period 1950 – 2014 and within the selected spatial domain (section 2.1.1) from ICOADS R3.0 have been used. This includes all ship based and drifting buoy observations. Those from moored buoys and other platforms have been excluded due to either a short period of record (e.g. Argo) or sparse point locations (e.g. moored buoys). In addition to ICOADS R3.0, global daily-mean sea surface temperatures, presented on a 0.05° latitude–longitude grid, with gaps between available daily observations filled by statistical means, spanning 1981 to 2016 from the ESA SST CCI SST version 2.0 product (SST CCI analysis, Good *et al.*, 2019; Merchant *et al.*, 2019) have been used to define covariances between grid cells (Section 2.3), estimate the sampling uncertainty (Section 2.2) and define the climatology.

2.1.2 | Spatial Domain and Selection of Data

The Atlantic Ocean in this dataset is as defined in the International Hydrographic Organization (IHO) publication S23, ‘Limits of oceans and Seas’ 3rd edition. Individual grid points are masked by this region and by the presence of data in the CCI SST gridded dataset. The extent of the grid covering the entire Atlantic Ocean is from 60°S to 68°N and 98°W to 20°E and the temporal coverage is from 1 January 1950 to 31 December 2014 with the first five-day period centred around mid-day GMT 3 January 1950. This produces a full grid of 256×236 points spatially, and 4,748 time steps. There are, in total, 33,080 grid cells per time step to interpolate and a total of 157,063,840 grid boxes. There are 83,536,825 observations from ships and drifting buoys in the region during the period occupying 22,790,841 grid boxes (14.5% of the total number of grid boxes) of which 14,291,205 have one single observation (63%) and 3,904,988 have two observations (17%). The maximum number of observations in a single grid cell is 1,121 from 10 individual buoys from a point in the middle of the North Atlantic (25.25°N , 37.75°W). We only used data from the ICOADS dataset if the trimming flag was less than or equal to 5.

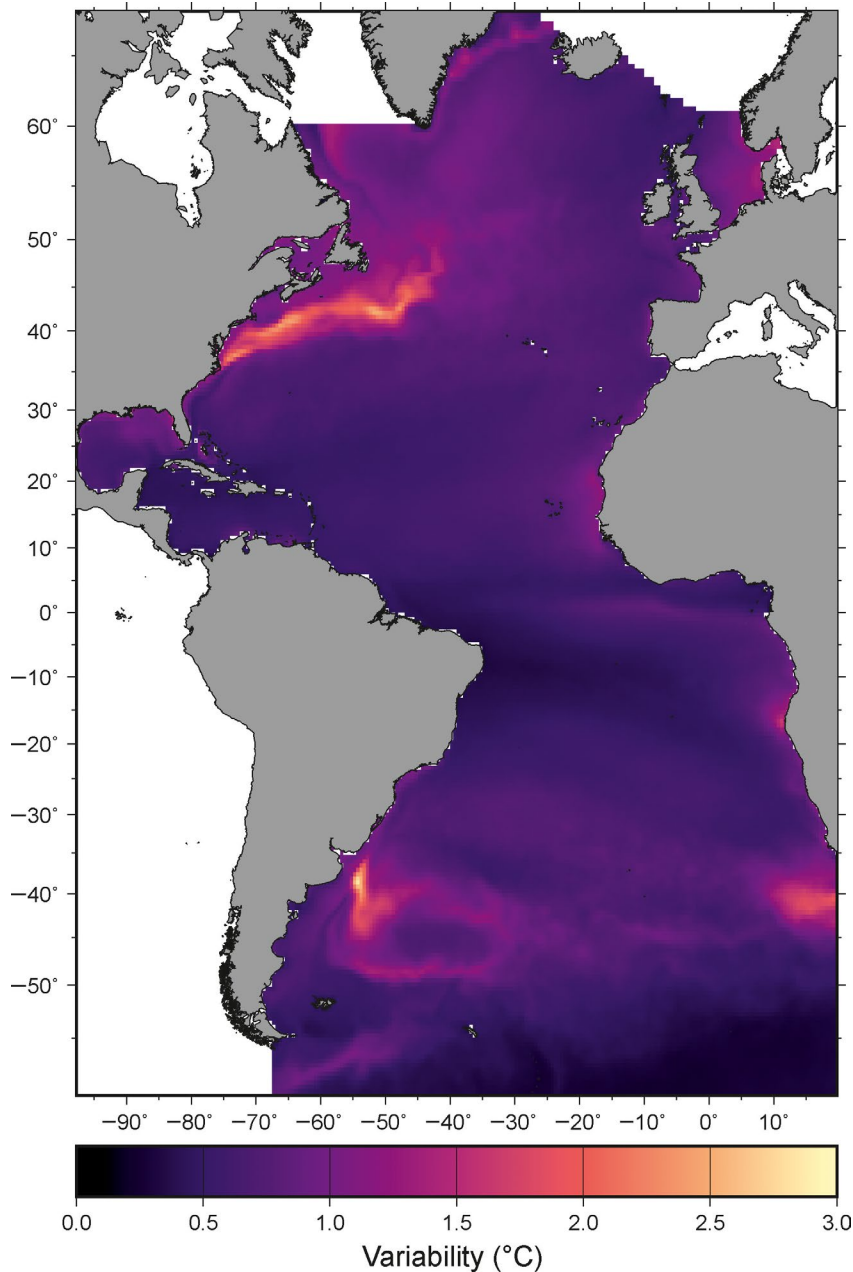


FIGURE 2 Regional Variability of SST for the Atlantic Region in terms of the standard deviation derived from the CCI SST analysis dataset

2.2 | Initial Gridding

2.2.1 | Calculation of Super-observations

For each grid box where there are data, we calculated the mean, median, trimmed mean (5th percentile at each end), sample standard deviation, sample trimmed standard deviation and interquartile range. The trimmed mean and sample standard deviations only differ from the mean and sample standard deviation if there are more than 10 observations in the grid box. Also recorded in the gridded ICOADS data file are the number of buoys and ships per grid box and the number of unique ships and buoys. These are useful if attempting to calculate the input data uncertainties.

The super-observations are then expressed as residuals from the 1981–2014 Climatology derived from the CCI SST

analysis. The climatology consists of a mean together with annual, semi-annual and tri-annual terms fitted using least squares. We chose to use the CCI SST analysis rather than from the ICOADS dataset itself because there are regions, especially the Southern Atlantic Ocean (Figure 1) where the data are too sparse to derive a good climatology. The climatology does not include the trend since it may not reflect that over the whole 1950–2014 period.

2.2.2 | Uncertainties

In order to interpolate the SST at global and regional levels, it is important to produce a realistic estimate of the observational uncertainties in the measurements. As discussed in

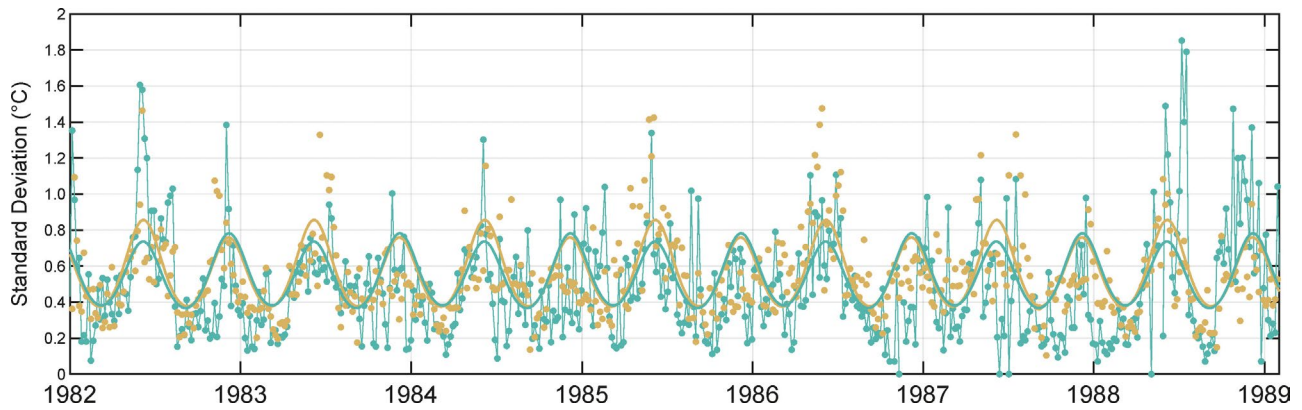


FIGURE 3 Example time series of the standard deviations from the ICOADS data (green dots and line) and the CCI data brown dots). Thick green and brown lines are the least-squares fit to the ICOADS and CCI data, respectively. Grid cell is point 54,501 in the Southern North Sea

Kennedy *et al* (2011a, 2014), the observational uncertainties are a product of three main errors; random measurement, bias and sampling errors. They estimated the measurement error to be 0.74°C and 0.26°C for ships and drifting buoys, respectively, and the bias error to be 0.71°C and 0.29°C for those platforms. We also performed several tests on the ICOADS data to derive estimates of the measurement and bias error. These included fits to the sample standard deviations as a function of the number of ships and buoys and unique ships and buoys per grid box, direct comparison with the CCI SST analysis for a small sample of grids with abundant data and examining the distribution of sample standard deviations from grid cells with there was either only one vessel or all the vessels were different. We estimate the uncertainties to be 1.47°C and 0.38°C for the ship and buoy bias error and 0.73°C and 0.24°C for the measurement errors, respectively. Our bias errors are larger than Kennedy *et al* (2011a) because individual measurement biases had not been removed from the ICOADS data prior to this (see Bias Reduction section below). This will imply that we are slightly cautious with our bias error when propagating to our observational uncertainties for the interpolation.

The sampling error is the error that arises when a finite number of observations are used to estimate a grid box average from a field that is spatially varying in that area. The sampling uncertainty term was given by Kennedy *et al* (2011a) by the following equation.

$$\sigma_{se}^2 = \frac{\sigma_s^2}{n} (1 - \bar{r}) \quad (1)$$

where n is the number of observations in a grid box; σ_s^2 is the variance of the SST anomalies at a point and assumed to be constant within a given grid box. \bar{r} is the average correlation between any two points within the grid box. Kennedy *et al* (2011a) calculated $\sigma_s^2 \bar{r}$ from grid boxes with very large n and estimated \bar{r} by calculating inter-grid box correlations and taking averages in space and combining these with their

equivalent time correlations. Here, we use the CCI SST analysis to derive $\sigma_s^2 (1 - \bar{r})$ by simply estimating the variance

from the intra-grid values. Since the CCI SST analysis is daily with a resolution of $1/20^{\text{th}}$ degree that gives $10 \times 10 \times 5$ values with which to calculate the variance in each grid box Figure 2. We note that estimating sampling uncertainty from the SST CCI analysis assumes that spatial variability at very small scales is correct. However, the SST CCI analysis already encodes assumptions about the small-scale spatial structure and its relationship to observational error in the satellite retrievals and therefore may bias the sample uncertainty estimates but we feel this is still a sensible approach to assigning sampling uncertainties for each grid box.

The sampling uncertainty from a single observation, $\sqrt{\sigma_s^2 (1 - \bar{r})}$, has a seasonal cycle, particularly in coastal zones, upwelling regions, fronts and narrow currents. We also see this in the ICOADS grids where we have a plentitude of data for example, Figure 3. To take this into account and extend the sampling uncertainty over the whole time frame of the dataset, we fit a climatology (mean, annual, semi-annual, tri-annual) to the CCI grid box variability and use this to derive our sampling uncertainty for the interpolation. Since the standard deviations are not normally distributed and to avoid producing anything negative, we fit the climatology in least squares assuming a log-normal distribution.

2.3 | Interpolation

Many methods have been used previously for reconstructing historical sea surface temperature records, including optimal interpolation (Lorenz, 1981; Reynolds and Smith, 1994) or Simple Kriging (Krige, 1951; Cressie, 1990); optimal smoothing,

Kalman Filter and reduced space optimal interpolation (Kaplan *et al.*, 1998); variational Bayesian principal component analysis (VBPCA; Ilin and Kaplan, 2009); and reduced space Kalman smoother (Karspeck *et al.*, 2012). Here, we use Simple Kriging, interpolating the super-observations calculated in 2.2.1. to estimate spatially complete fields of the SST. As part of the Kriging process, the mean field is subtracted from the super-observations by subtracting the climatological mean to give anomalies. These are then interpolated by using Equations 2 and 3:

$$z_k = CH^T (HCH^T + HRH^T)^{-1} Hd \quad (2)$$

and

$$C_{z_k} = C - CH^T (HCH^T + HRH^T)^{-1} HC \quad (3)$$

Where z_k are the interpolated values, and their covariance (C_{z_k}), over the whole grid, C is the spatial covariance of the signal, R is a diagonal matrix (nominally, if disregarding observational correlations,) of the estimated variances of the errors in the observations, H is a matrix that maps the data for a given epoch to the full set of grid points, and d is the full vector of climatology-removed observations (0 for missing observations). The spatial covariance terms C have been estimated using the ESA CCI SST analysis data. Rather than estimating the spatial covariances using a parametric approach, for example using variograms, we have estimated the covariance between grid boxes directly from the ESA CCI SST analysis data. Figure 4 illustrates the range in variation in the cross-correlation for three points in the Atlantic Ocean derived from the ESA CI SST derived covariance. A point in the vicinity of the Gulf Stream (Figure 4, middle) has a smaller correlation distance than the other two points. This is similar to the approach taken by Church *et al.* (2004) when reconstructing global sea level using tide gauges and a satellite altimetry field. In this dataset, we have ignored inter-grid observational correlations in R simply because we assert that given the temporal scale used and that we are interpolating spatially, the correlations would have a negligible effect in the interpolation. However, note that intra-grid correlations are accounted for via the methodology described below. We can take two approaches here to estimate the variance of the super-observations calculated in 2.2.1. First, we can calculate a theoretical uncertainty based on the values derived in 2.2.2 and using the equation (adapted from Kennedy *et al.*, 2011a equation 8).

$$\begin{aligned} \sigma_{err}^2 &= \frac{1}{n} \left(\frac{n_s \sigma_{m_{ship}}^2 + n_b \sigma_{m_{buoy}}^2}{n_s + n_b} \right) \\ &+ \frac{1}{n^2} \left(\frac{n_s^2}{m_s} \sigma_{b_{ship}}^2 + \frac{n_b^2}{m_b} \sigma_{b_{buoy}}^2 \right) \\ &+ \frac{1}{n} \sigma_s^2 (1 - \bar{r}) \end{aligned} \quad (4)$$

where n_s and n_b ($n_s + n_b = n$) are the number of ship and buoy measurements in a grid box and m_s and m_b are the number of ships and buoys in a grid box. Also $\sigma_{m_{ship}}$ and $\sigma_{m_{buoy}}$ are the ship and buoy measurement uncertainties and $\sigma_{b_{ship}}$ and $\sigma_{b_{buoy}}$ are the bias uncertainties. For simplicity, this assumes that each of the m ships and buoys makes the same number of observations in the grid box and the measurement and bias uncertainties are the same for all ships and buoys.

A second approach is to use the sample standard deviations (or the trimmed sample standard deviations) as these reflect the true variations in the observations. If the error came from just one source, then we would calculate the uncertainty of the observation as

$$\sigma_{err}^2 = \frac{1}{n} \sigma_{sample}^2 \quad (5)$$

where σ_{sample}^2 is the sample standard deviation. However,

where there are more than one source of noise, and these depend on the number of ships, buoys and the number of measurements; this is too simplistic. In addition, where the sample sizes are small, the sample standard deviations are likely to be biased (Cochran, 1934) or not quantifiable if there is only one observation in the grid cell. Therefore, we take a hybrid approach to estimating the measurement uncertainties. For grid cells with only one or two observations, we use the estimates from Equation 4. For all other grid cells, we calculate a predicted sample standard deviation using the measurement, bias and sample uncertainties and taking care of biases due to small sample sizes. If a grid cell sample standard deviation is less than the predicted value, we use the estimates from Equation 4. If it is larger, then we take the ratio of the predicted sample standard deviation and Equation 4 and scale the sample standard deviation by this ratio.

2.4 | Bias reduction

As noted in section 2.1.1, the SST observations contain biases and prior authors have developed bias corrections to reduce the impacts of these biases. Rather than developing a new bias correction, we have interpolated the bias correction from the HadSST.0.0.0 dataset (Kennedy *et al.*, 2019) to our analysis grid. The bias correction was derived by taking the difference between the median and the unadjusted SST anomalies grids (HadSST.4.0.0.0_median.nc and HadSST.4.0.0.0_unadjusted.nc). This interpolated bias adjustment has then been subtracted from the super-observations to give a bias-adjusted dataset.

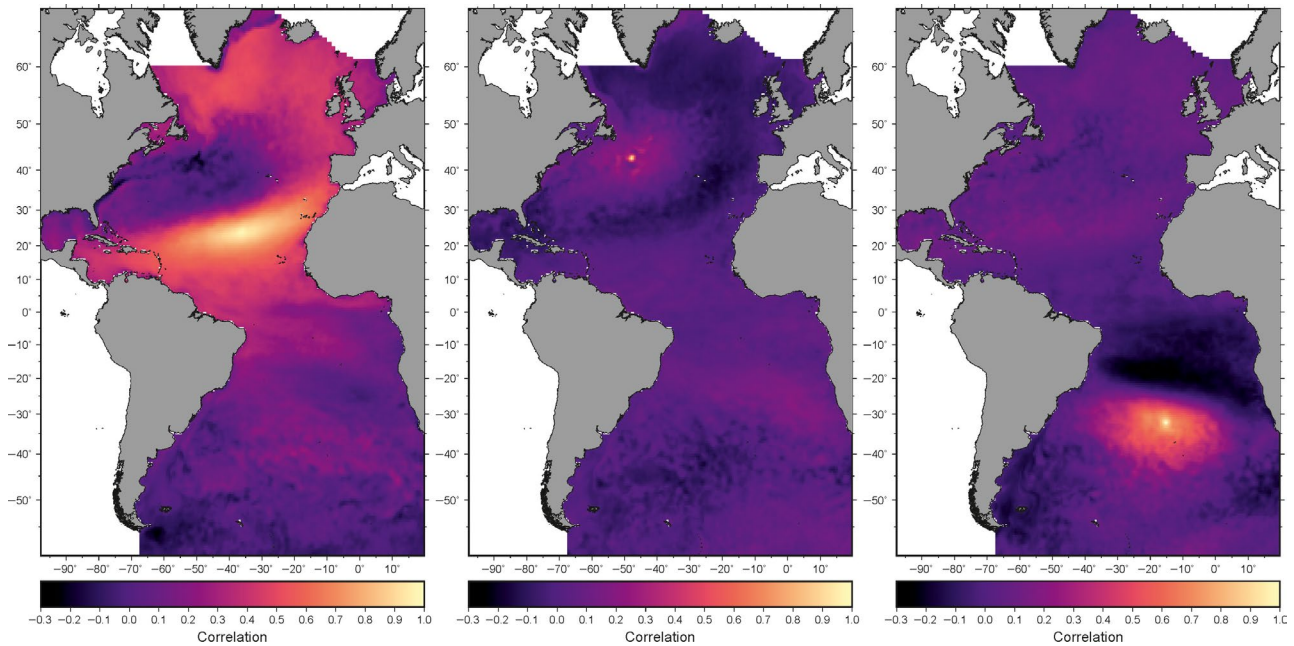


FIGURE 4 Correlation for three grid points in the Atlantic Ocean. Left, central North Atlantic; middle, in the vicinity of the Gulf Stream; right, central South Atlantic

2.5 | Verification

To validate the data, we again use the SST CCI analysis dataset. Figure 5 shows a map of mean absolute error (MAE) for the differences between our interpolated results and the CCI SST analysis residuals (CCI SST analysis minus the climatology). We calculate an overall mean absolute error of 0.39°C . We also calculate the MAE for the whole region as a function of time step (Figure 6). The MAE has gradually reduced from around 0.45°C in the early 1980s to about 0.35°C now. We also examined the correlation and coherence between the two datasets both spatially and temporally (Figure 7). The magnitude squared coherence (Stoica and Moses, 2005) acts as a form of correlation in the frequency domain. We see that the spatially averaged coherence between the two datasets increases at longer periods (Figure 7). The obvious drops in coherence are at the annual and its harmonics which are expected because the climatology has been removed from both sets. The increasing correlation at longer periods can also be seen in the middle panels of Figure 7 which show averaged coherence at low, median and high frequencies. Lower coherence between the two datasets at shorter periods is to be expected for several reasons. First, the power-law nature of many geophysical series (Agnew, 1992) including SST (e.g. Bürgert and Hsieh, 1989) means that the largest signals are at the longest periods and are likely to have the highest correlation. Secondly, random measurement noise will manifest itself more at higher frequencies for the same reason as above, reducing the correlations at short periods. Finally, the CCI SST analysis is subject to some degree of

smoothing when infilling gaps in observations (Merchant *et al.*, 2019). This again will be at short periods and wavelengths, reducing the correlation there. Overall the correlation (Figure 7, top right) is greatest in the Northern Atlantic Ocean except in the region of the gulf stream. It is not necessarily where the data is the densest (Figure 1) but tracks more where the SST variation is lowest (Figure 2). However, in the Southern Atlantic Ocean, the lower correlation outside of the regions of high variability is probably due to data density. Overall the correlation has increased over time from the start of the CCI dataset to the present (Figure 7, bottom). Finally, note that Figure 7 top right and middle left are similar since they both reflect the low-frequency correlation. However, Figure 7 top left is the Pearson correlation coefficient calculated in the time domain and the coherence in Figure 7 middle left is calculated in the spectral domain.

Figure 8(top) shows a map of the uncertainty averaged over 1950 – 2014. Over the majority of the ocean, the uncertainty is in the range $0.2\text{--}0.4^{\circ}\text{C}$, increasing to over 1°C in the high variability regions. Figure 8(bottom) shows the time series of the spatially averaged uncertainty over the same period. The uncertainty decreases from $\sim 0.45^{\circ}\text{C}$ during the 1950s to just over 0.3°C by 2014. The impact of the drifting buoy network can be seen in the mid-2000s, with a sharp decrease in the uncertainty.

Figure 9 shows the mean anomaly (w.r.t. 1981–2014) for a sample month (January 1963) from HadSST4.0.0.0, ERSST5 (Huang *et al.*, 2017) and the new dataset at their native spatial resolutions, 5° , 2° and 0.5° , respectively. Also shown are the products averaged or interpolated to

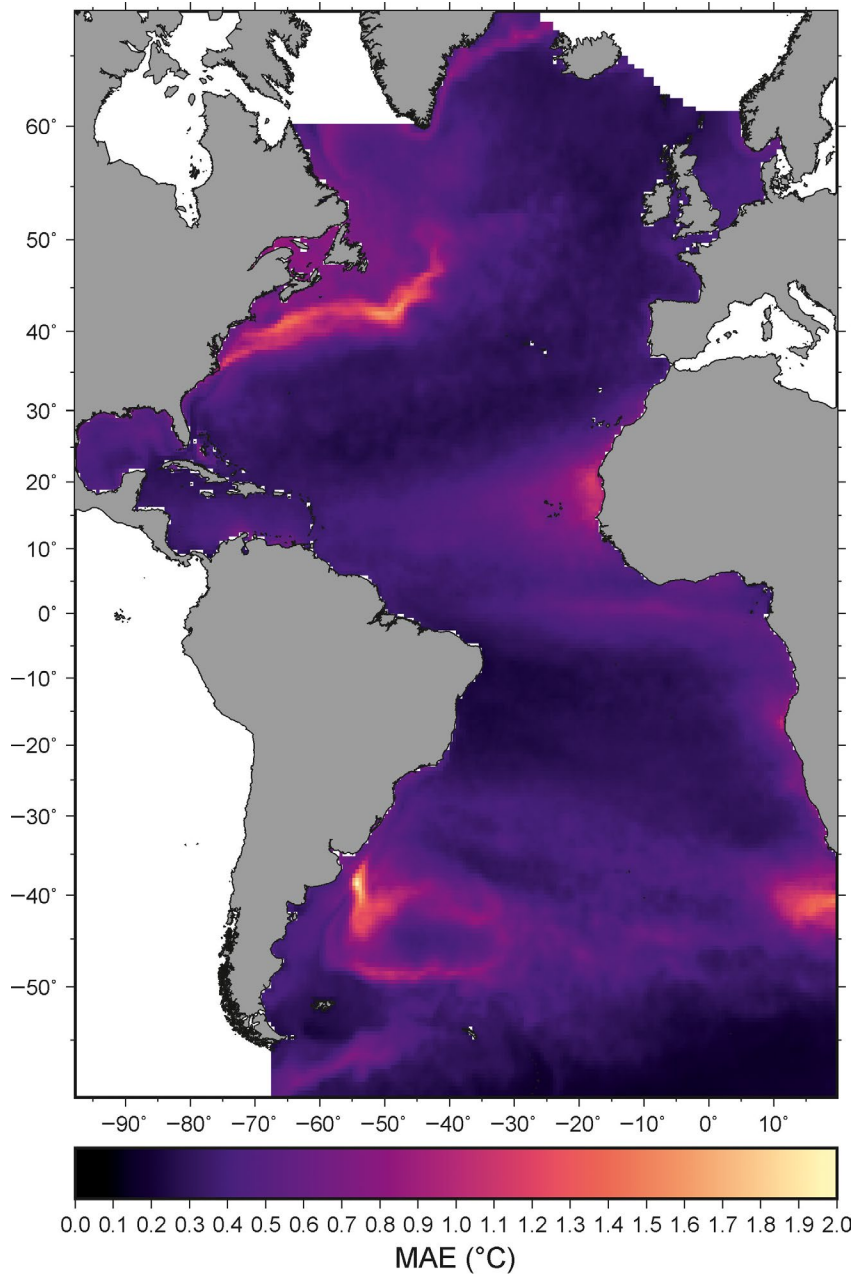


FIGURE 5 Map of mean absolute error between the ICOADS interpolated and the CCI SST analysis residuals

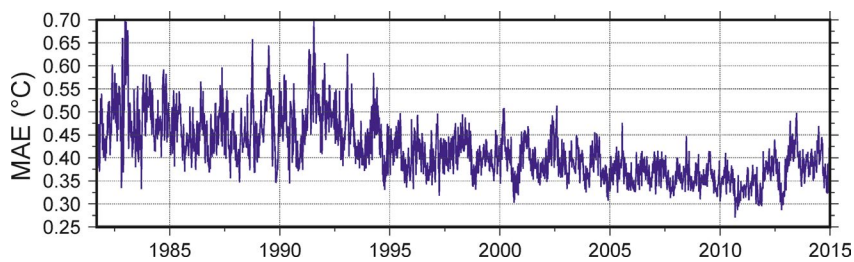


FIGURE 6 Mean absolute error between the ICOADS interpolated residuals and the CCI SST analysis residuals as a function of time

the other resolutions. In general, good agreement is seen between the different products but with some differences. These are expected due to different gridding methods and/or bias adjustments. The increased spatial variability and finer structures are clearly visible in the new product. Figure 10 shows a time series of the spatially averaged

anomaly (w.r.t 1981–2014) for the three datasets. Again, there is generally good agreement overall but with differences between individual time periods.

To validate the estimated (formal) uncertainties derived from Equation 4, we split the grids into groups depending on the formal uncertainty size in steps of 0.2°C and then

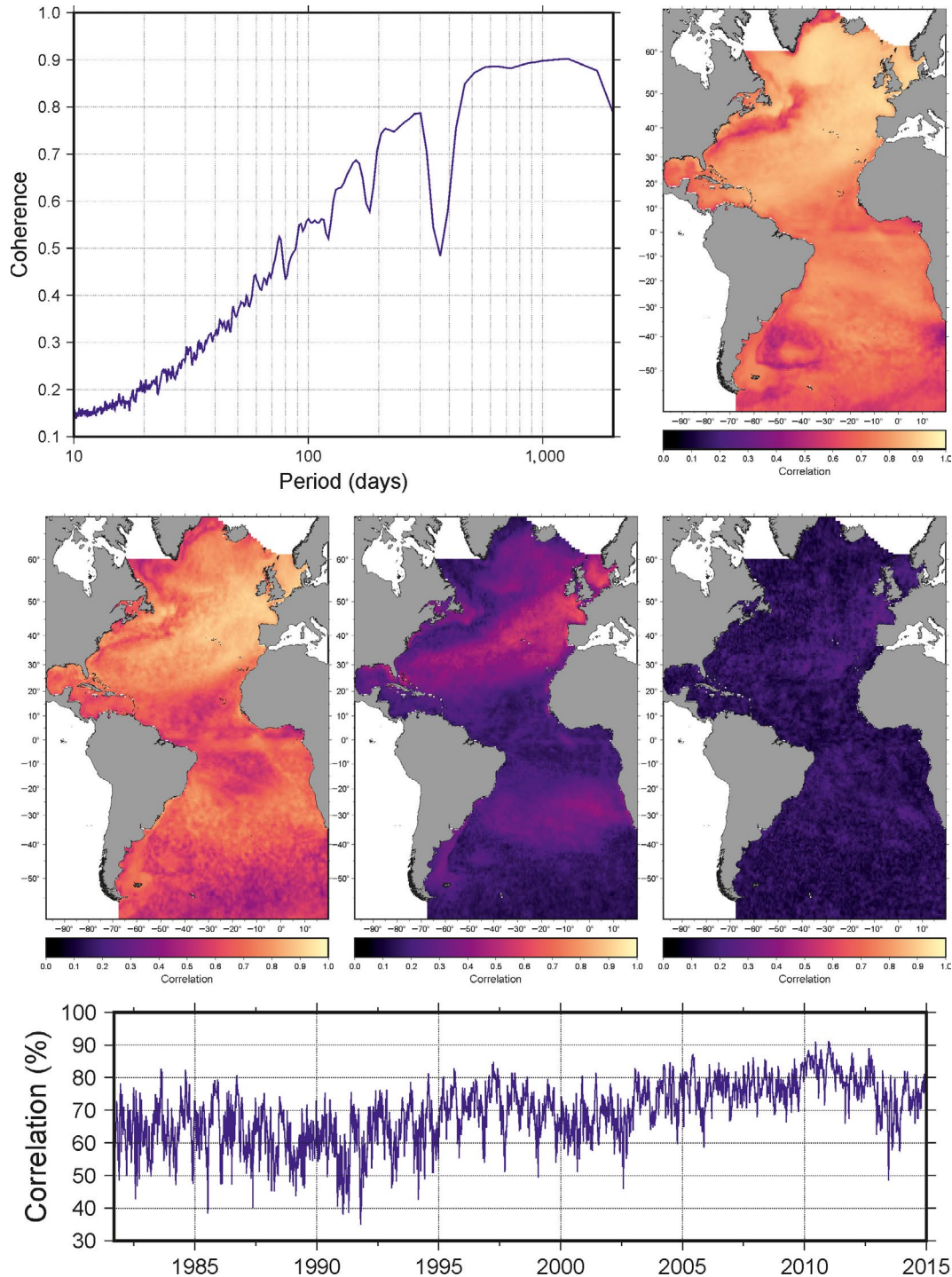


FIGURE 7 Comparison of ICOADS interpolated SST and CCI SST analysis. Top left, average coherence as a function of period showing increasing coherence with period except at annual and its harmonics, which we removed from both. Top right, Pearson correlation coefficient for each grid cell. Middle panels, average correlation for long (left, 100–5,000 days), median (middle, 18–22 days) and short (right, 10–11 days) periods. Bottom, average correlation as a function of time

produced boxplots for the differences between this dataset and the CCI SST analysis (Figure 11). We use Tukey style whiskers ($1.5 \times$ interquartile range, IQR) past the 25th to 75th percentile boxes. The increasing spread with increasing formal uncertainty validates those uncertainties. Overall, if we take the differences and divide by the formal uncertainties,

we find that the uncertainties slightly conservative with a median value of 1.4. The formal uncertainties should therefore be scaled by 1.4 to be more realistic.

As a final test to validate the performance of the interpolation where grid cells had no super-observations, we performed an internal test with the CCI SST analysis only. Here,

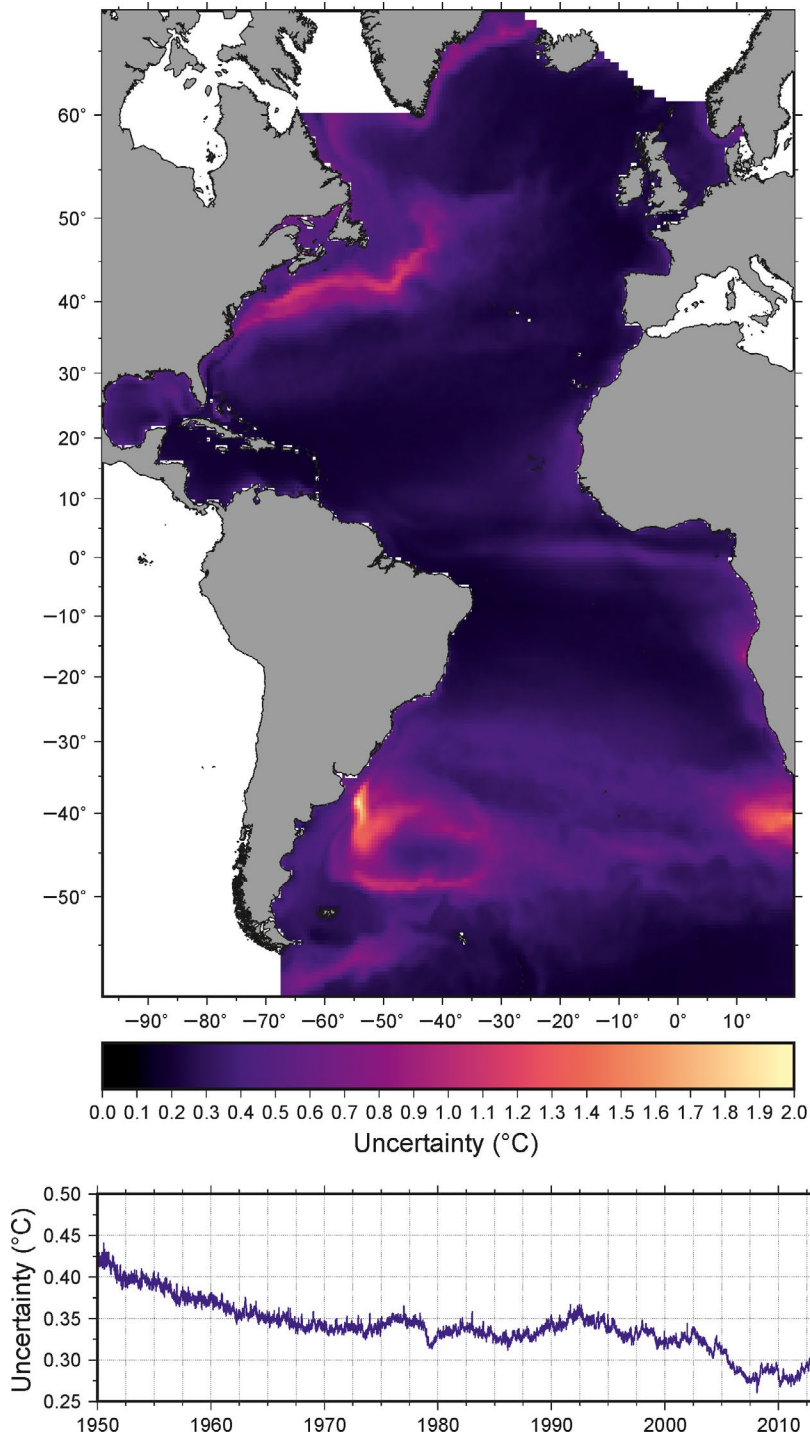


FIGURE 8 Mean uncertainty in ICOADS interpolated SST (top) over 1950–2014 and (bottom) spatially averaged over the Atlantic Ocean

we sampled the CCI SST data at the times and positions of the ICOADS measurements and then interpolated these in the same way as before. We then took all the grid cells that had no super-observations and compared the interpolated with the actual CCI SST values (Figure 12). Similar to Figure 11, we split the comparison as a function of the formal uncertainties. The scatter plots are colour-coded based on the density of the points in the region. Points with a density of less than 1,000 per $^{\circ}\text{C}$ are removed for clarity. We find good correlation (0.95) between the interpolated values and the CCI data for unsampled

regions for the formal uncertainties of between 0 and 0.2°C . As the formal uncertainties increase, the correlation decreases and is indicative of a slight reduction in the magnitude of the anomalies. We acknowledge that we are pushing the boundaries with these resolutions especially in data sparse regions such as the Southern Hemisphere. However, we are still confident that the results are useful. Figure 13 is an example of a point in the Southern Atlantic Ocean with low correlation (0.56) and a small number (26) of observations. The fit is still good, particularly at long wavelengths.

FIGURE 9 Monthly mean SST anomaly for January 1963 (w.r.t 1981–2014) for HadSST4 (left column), ERSST5 (middle column) and this dataset (right column) at native resolution and averaged to the resolution of the other datasets

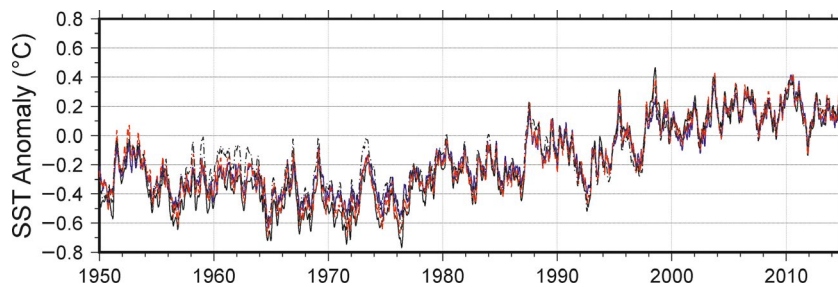
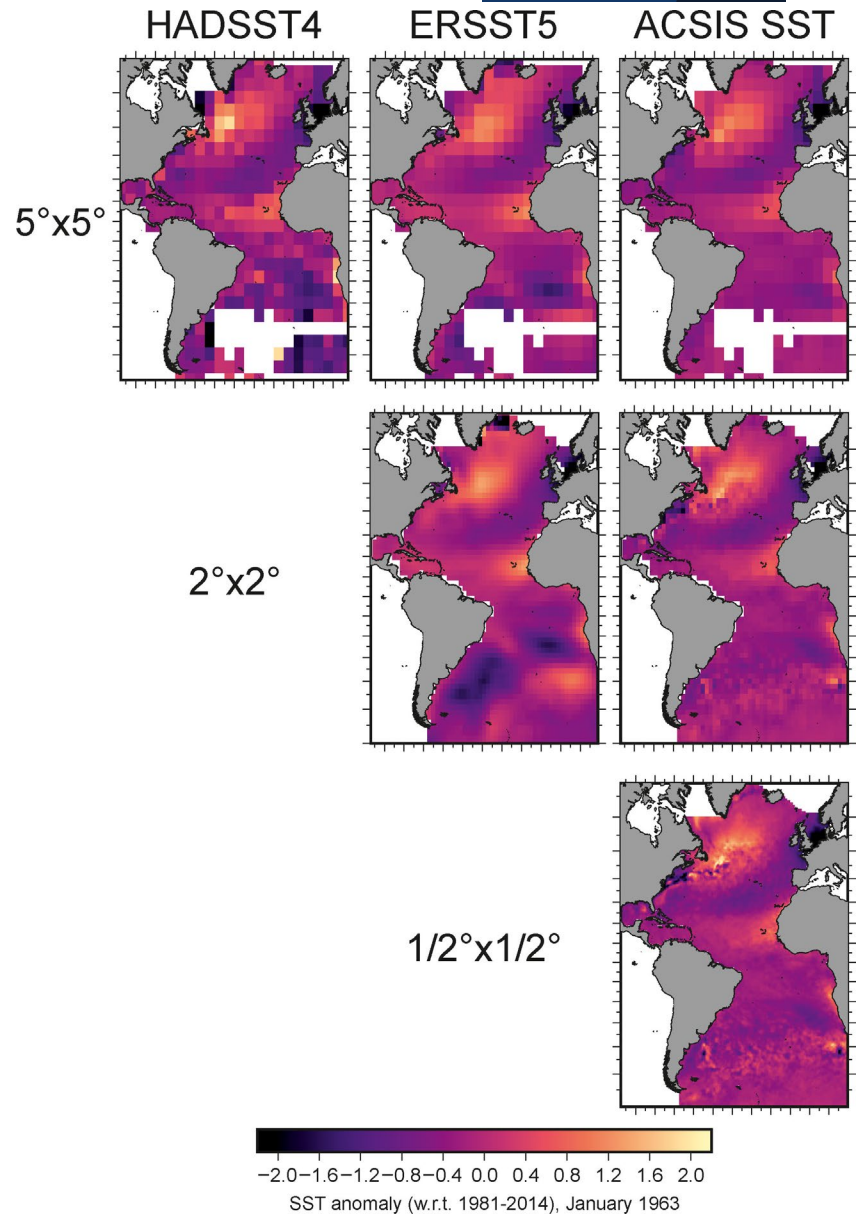


FIGURE 10 Spatially averaged SST anomalies over Atlantic Ocean for HadSST4 (solid black), ERSST5 (dotted black) and this dataset (red dashed). HadSST4 and ERSST5 have been interpolated to the same grid as the new estimates (0.5° , 5 day) prior to averaging and only grid cells with estimates in all 3 datasets used. For comparison, the spatially complete values for the new dataset are also shown in blue. A 6-point running mean filter has been applied to all time series for clarity

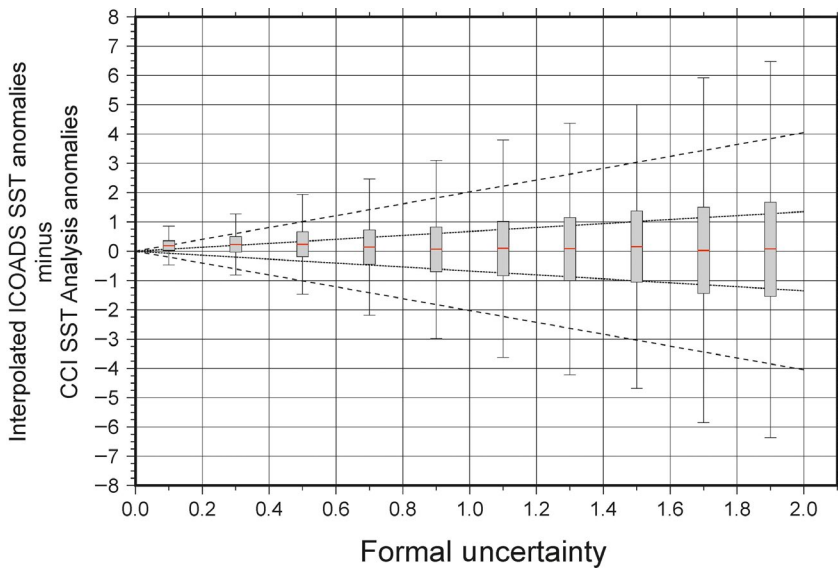


FIGURE 11 Box plot of the ICOADS interpolated SST minus CCI SST analysis as a function of the derived formal uncertainty. Red lines indicate the median, box indicates the 25th to 75th percentile, and the whiskers are Tukey style ($1.5 \times \text{IQR}$) beyond the percentiles. Dotted lines indicate the expected 25th and 75th percentile based on the formal uncertainty. Dashed lines indicate the predicted $1.5 \times \text{IQR}$

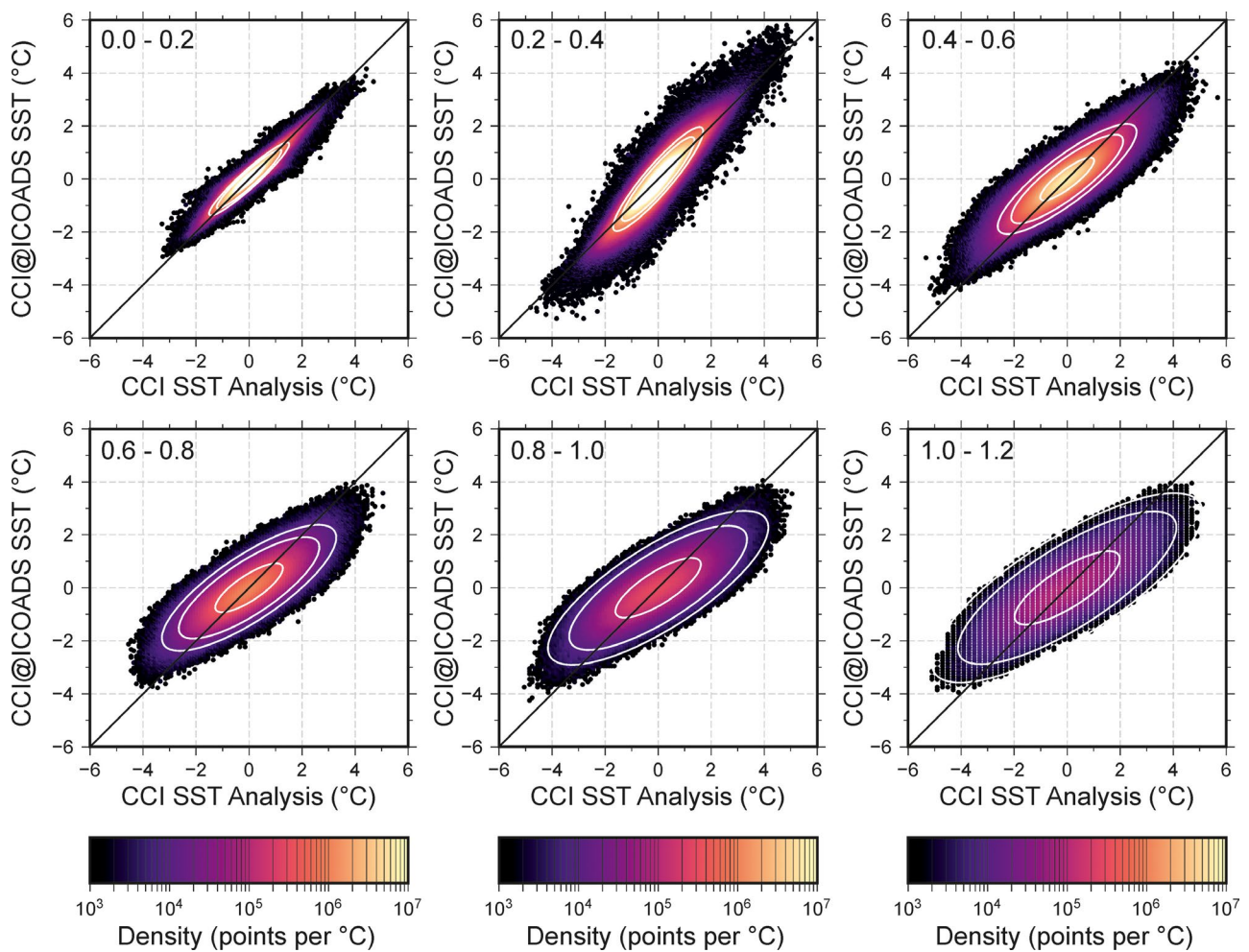


FIGURE 12 Scatter plots of CCI SST analysis estimates mapped to ICOADS measurement times and positions and then interpolated as for the dataset versus the CCI SST analysis. Only grid cells that do not include ‘observations’ are included. Colours represent the density of points in the region. Points where the density is less than 1,000 points per $^{\circ}\text{C}$ are removed for clarity. The white ellipses are the 50th, 95th and 99th percentiles derived from the estimated covariance between the two datasets. The results have been partitioned as a function of the formal uncertainties (range given in the top left of each plot)

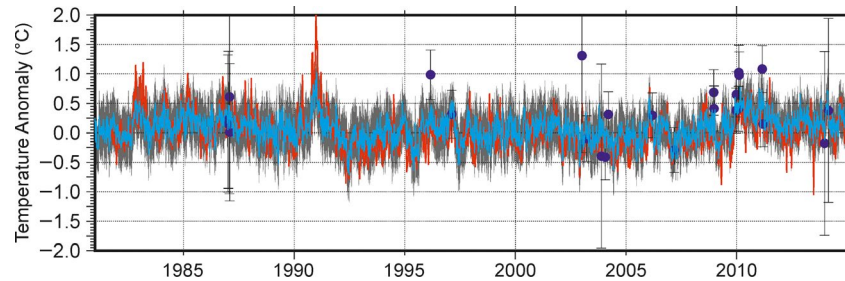


FIGURE 13 Temperature anomaly time series for a point (S 53.25, E 10.25) in the Southern Atlantic Ocean. Blue dots are the ICOADS super-observations for this grid point. Cyan line and grey region (2 sigma error) are the interpolated ICOADS anomalies. Red line is the CCI SST analysis

3 | DATASET LOCATION AND FORMAT

The dataset is available from the Centre for Environmental Data Analysis (CEDA) archive in annual CF compliant NetCDF files, with a total of 65 annual files are available. Each file contains: the 5-day mean sea surface temperature; the corresponding climatological value, the sea surface temperature anomaly and the uncertainty in the sea surface temperature. The data are freely open and available with no restrictions on use but prior registration is required to download the data. More information on the CEDA archive and access to the data can be found at <http://archive.ceda.ac.uk/>

4 | DATASET USE AND REUSE

The new dataset presented in this paper has been developed as part of the UK North Atlantic Climate System Integrated Study (ACSIS) for use in validating and comparing with regional climate models. Other potential uses include boundary forcing for regional re-analyses, monitoring and assessment of regional climate change and other studies requiring SST at a resolution higher than typical for the in situ products (i.e. <1 month, $<1^\circ$) and spanning the satellite and presatellite era. Future plans for the dataset include updating to use the ICOADS NRT updates once the known issues have been resolved and investigation of whether a resolution of 0.25° daily is feasible with the in situ data.

ACKNOWLEDGEMENTS

The research presented in this paper was funded by the UK Natural Environment Research Council 'The North Atlantic Climate System Integrated Study (ACSIS)' grant, reference NE/N018044/1. The authors are grateful to Dr Elizabeth Kent for advice and discussion of the methods used and approach to bias adjustment and Dr John Kennedy for making the bias adjustments applied to the HadSST.4.0.0.0 dataset available.

ORCID

Simon David Paul Williams  <https://orcid.org/0000-0003-4123-4973>

David I. Berry  <https://orcid.org/0000-0002-3862-3479>

REFERENCES

- Agnew, D.C. (1992) The time-domain behavior of power-law noises. *Geophysical Research Letters*, 19(4), 333–336.
- Blunden, J., Arndt, D.S. (2019) State of the climate in 2018. *Bulletin of the American Meteorological Society*, 100(9), Si–S306.
- Bojinski, S., Verstraete, M., Peterson, T.C., Richter, C., Simmons, A. and Zemp, M. (2014) The concept of essential climate variables in support of climate research, applications, and policy. *Bulletin of the American Meteorological Society*, 95(9), 1431–1443. <https://doi.org/10.1175/bams-d-13-00047.1>
- Bürgert, R. and Hsieh, W.W. (1989) Spectral analysis of the AVHRR sea surface temperature variability off the west coast of Vancouver Island. *Atmosphere-Ocean*, 27(3), 577–587. <https://doi.org/10.1080/07055900.1989.9649354>
- Carella, G., Kent, E.C., Berry, D.I., Morak-Bozzo, S. and Merchant, C.J. (2017) Measurements and models of the temperature change of water samples in sea surface temperature buckets. *Quarterly Journal of the Royal Meteorological Society*, 143(706), 2198–2209. <https://doi.org/10.1002/qj.3078>
- Chan, D. and Huybers, P. (2019) Systematic differences in bucket sea surface temperature measurements among nations identified using a linear-mixed-effect method. *Journal of Climate*, 32(9), 2569–2589. <https://doi.org/10.1175/JCLI-D-18-0562.1>
- Church, J.A., White, N.J., Coleman, R., Lambeck, K. and Mitrovica, J.X. (2004) Estimates of the regional distribution of sea level rise over the 1950–2000 period. *Journal of Climate*, 17(13), 2609–2625. [https://doi.org/10.1175/1520-0442\(2004\)017<2609:Eotrd>2.0.Co;2](https://doi.org/10.1175/1520-0442(2004)017<2609:Eotrd>2.0.Co;2)
- Cochran, W.G. (1934) The distribution of quadratic forms in a normal system, with applications to the analysis of covariance. *Mathematical Proceedings of the Cambridge Philosophical Society*, 30(2), 178–191. <https://doi.org/10.1017/S030500410001659>
- Cressie, N. (1990) The Origins of Kriging. *Mathematical Geology*, V22(3), 239–252. <https://doi.org/10.1007/BF00889887>
- Dee, D.P., Uppala, S.M., Simmons, A.J., Berrisford, P., Poli, P., Kobayashi, S. *et al.* (2011) The ERA-Interim reanalysis: configuration and performance of the data assimilation system. *Quarterly Journal of the Royal Meteorological Society*, 137(656), 553–597. <https://doi.org/10.1002/qj.828>

- Flato, G., Marotzke, J., Abiodun, B., Braconnot, P., Chou, S.C., Collins, W. *et al.* (2013). Evaluation of Climate Models. In: Stocker, T., Qin, D., Plattner, G.K., Tignor, M., Allen, S.K., Boschung, J., Nauels, A., Xia, Y., Bex, V. and Midgley, P.M. (eds). *Climate Change 2013: The Physical Science Basis. Contribution of Working Group I to the Fifth Assessment Report of the Intergovernmental Panel on Climate Change*, Cambridge, UK and New York, NY: Cambridge University Press, pp. 741–866. <https://doi.org/10.1017/CBO9781107415324.020>
- Freeman, E., Woodruff, S.D., Worley, S.J., Lubker, S.J., Kent, E.C., Angel, W.E. *et al.* (2017) ICOADS Release 3.0: a major update to the historical marine climate record. *International Journal of Climatology*, 37(5), 2211–2232. <https://doi.org/10.1002/joc.4775>
- Freeman, E., Kent, E.C., Brohan, P., Cram, T., Gates, L., Huang, B. *et al.* (2019) The international comprehensive ocean-atmosphere data set – Meeting users needs and future priorities. *Frontiers in Marine Science*, 6, 435. <https://doi.org/10.3389/fmars.2019.00435>
- Good, S.A., Embury, O., Bulgin, C.E. and Mittaz, J. (2019): *ESA Sea Surface Temperature Climate Change Initiative (SST_cci): Level 4 Analysis Climate Data Record, version 2.0*. Centre for Environmental Data Analysis, 22 August 2019. <https://doi.org/10.5285/aced40d7cb964f23a0fd3e85772f2d48>
- Hirahara, S., Ishii, M. and Fukuda, Y. (2014) Centennial-scale sea surface temperature analysis and its uncertainty. *Journal of Climate*, 27(1), 57–75. <https://doi.org/10.1175/jcli-d-12-00837.1>
- Huang, B., Thorne, P.W., Banzon, V.F., Boyer, T., Chepurin, G., Lawrimore, J.H. *et al.* (2017) Extended reconstructed sea surface temperature, Version 5 (ERSSTv5): Upgrades, validations, and intercomparisons. *Journal of Climate*, 30(20), 8179–8205. <https://doi.org/10.1175/jcli-d-16-0836.1>
- Ilin, A. and Kaplan, A. (2009) Bayesian PCA for reconstruction of historical sea surface temperatures. *International Joint Conference on Neural Networks*, 1–6, 1138–1143.
- IPCC, (2014). *Climate Change 2014: Synthesis Report*. In Core Writing Team, Pachauri, R.K. and Meyer, L.A. (eds.). *Contribution of Working Groups I, II and III to the Fifth Assessment Report of the Intergovernmental Panel on Climate Change*. Geneva, Switzerland: IPCC, p. 151.
- Kaplan, A., Cane, M.A., Kushnir, Y., Clement, A.C., Blumenthal, M.B. and Rajagopalan, B. (1998) Analyses of global sea surface temperature 1856–1991. *Journal of Geophysical Research-Oceans*, 103(C9), 18567–18589. <https://doi.org/10.1029/97jc01736>
- Karspeck, A.R., Kaplan, A. and Sain, S.R. (2012) Bayesian modeling and ensemble reconstruction of mid-scale spatial variability in North Atlantic sea-surface temperatures for 1850–2008. *Quarterly Journal of the Royal Meteorological Society*, 138(662), 234–248. <https://doi.org/10.1002/qj.900>
- Kennedy, J.J. (2014) A review of uncertainty in in situ measurements and data sets of sea surface temperature. *Reviews of Geophysics*, 52, 1–32. <https://doi.org/10.1002/2013RG000434>
- Kennedy, J.J., Rayner, N.A., Smith, R.O., Parker, D.E. and Saunby, M. (2011a) Reassessing biases and other uncertainties in sea surface temperature observations measured in situ since 1850: 1. Measurement and sampling uncertainties. *Journal of Geophysical Research*, 116, D14103. <https://doi.org/10.1029/2010JD015218>
- Kennedy, J.J., Rayner, N.A., Smith, R.O., Saunby, M., Parker, D.E. (2011b) Using AATSR data to assess the quality of in situ sea-surface temperature observations for climate studies. *Remote Sensing of Environment*, 2, 79–92. <https://doi.org/10.1029/2010JD015220>
- Kennedy, J.J., Rayner, N.A., Atkinson, C.P. and Killick, R.E. (2019) An ensemble data set of sea-surface temperature change from 1850: the Met Office Hadley Centre HadSST.4.0.0.0 data set. *Journal of Geophysical Research: Atmospheres*, 124, 7719–7763. <https://doi.org/10.1029/2018JD029867>.
- Kent, E.C., Woodruff, S.D. and Berry, D.I. (2007) Metadata from WMO publication no. 47 and an assessment of voluntary observing ship observation heights in ICOADS. *Journal of Atmospheric and Oceanic Technology*, 24, 214–234. <https://doi.org/10.1175/JTECH1949.1>.
- Kent, E.C., Kennedy, J.J., Smith, T.M., Hirahara, S., Huang, B., Kaplan, A. *et al.* (2017) A call for new approaches to quantifying biases in observations of sea surface temperature. *Bulletin of the American Meteorological Society*, 98, 1601–1616. <https://doi.org/10.1175/BAMS-D-15-00251.1>.
- Krige, D.G. (1951) A statistical approach to some basic mine valuation problems on the Witwatersrand. *Journal of the Southern African Institute of Mining and Metallurgy*, 52(6), 119–139.
- Lindstrom, E., Gunn, J., Fischer, A., McCurdy, A. and Glover, L.K., Task Team for the Integrated Framework for Sustained Ocean Observing (2012) *A Framework for Ocean Observing*. Paris France: UNESCO, p. 25. (IOC Information Document 1284, Rev. 2). <https://doi.org/10.5270/OceanObs09-FOO>.
- Lorenc, A.C. (1981) A global 3-dimensional multivariate statistical interpolation scheme. *Monthly Weather Review*, 109(4), 701–721.
- Merchant, C.J., Embury, O., Roberts-Jones, J., Fiedler, E., Bulgin, C.E., Corlett, G.K. *et al.* (2014) Sea surface temperature datasets for climate applications from Phase 1 of the European Space Agency Climate Change Initiative (SST CCI). *Geoscience Data Journal*, 1(2), 179–191. <https://doi.org/10.1002/gdj3.20>.
- Merchant, C.J., Embury, O., Bulgin, C.E., Block, T., Corlett, G.K., Fiedler, E. *et al.* (2019) Satellite-based time-series of sea-surface temperature since 1981 for climate applications. *Scientific Data*, 6(1), 223. <https://doi.org/10.1038/s41597-019-0236-x>.
- Rayner, N.A., Parker, D.E., Horton, E.B., Folland, C.K., Alexander, L.V., Rowell, D.P. *et al.* (2003) Global analyses of sea surface temperature, sea ice, and night marine air temperature since the late nineteenth century. *Journal of Geophysical Research: Atmospheres*, 108(D14), 4407. <https://doi.org/10.1029/2002jd002670>.
- Reynolds, R.W. and Smith, T.M. (1994) Improved global sea surface temperature analyses using optimum interpolation. *Journal of Climate*, 7(6), 929–948.
- Stoica, P. and Moses, R. (2005) *Spectral Analysis of Signals*. Upper Saddle River, NJ: Prentice Hall.
- Villegas-Hernández, H., Lloret, J. and Muñoz, M. (2015) Climate-driven changes in life-history traits of the bastard grunt (*Pomadasys incisus*) in the north-western Mediterranean. *Mediterranean Marine Science*, 16(1), 21–30. <https://doi.org/10.12681/mms.951>.

How to cite this article: WilliamsSDP, Berry DI. ACSIS Atlantic Ocean medium resolution SST dataset: Reconstructed 5-day, ½-degree, Atlantic Ocean SST (1950-2014). *Geosci. Data J.* 2020;00:1–14. <https://doi.org/10.1002/gdj3.94>